





PAPER

A new approach to radiochromic film dosimetry based on non-local means

César Rodríguez^{1,2} , Alfonso López-Fernández^{1,2} and Diego García-Pinto² ¹ Medical Physics and Radiation Protection Service, Fuenlabrada University Hospital, Fuenlabrada, Spain² Medical Physics, Radiology Department, Complutense University, Madrid, SpainE-mail: cesar.rodriguez@salud.madrid.org**Keywords:** film dosimetry, radiochromic film, Gafchromic EBT3, flatbed scanner, non-local means**Abstract**

Radiochromic film in conjunction with flatbed scanners are frequently employed as dosimeters for advanced techniques in radiotherapy. Their strengths are as follows: light element composition, low energy dependence, near biological tissue equivalence and high spatial resolution. However, they have some weaknesses as well: non-uniformities, read out noise, and scanning artifacts. Several processing protocols have been proposed intending to correct the perturbations these weaknesses produce. The aim of this paper is to present a new processing protocol for radiochromic film dosimetry based on a non-local means denoising algorithm. Three dose distributions of open square fields and a spatial combination of these fields using different angles of incidence and monitor units have been employed to validate the protocol. The dose distributions are traceable to ionization chamber measurements. Additionally, a real dose distribution of a treatment was used to simulate scanning data with noise and scanning lateral artifact, and to study how the protocol behaves under these perturbations. The same measured raw data have been processed by means of an implementation of the multichannel protocol (multigaussian method). It has been found that the proposed protocol reduces dose uncertainty even though it uses fewer scans than the multichannel protocol.

1. Introduction

Radiochromic films are suitable 2D radiation detectors for advanced techniques in radiotherapy due to their composition based on light elements, low energy dependence, near biological tissue equivalence and high spatial resolution (Niroomand-Rad *et al* 1998, Villarreal-Barajas and Khan 2014, Devic *et al* 2016). Furthermore, current Gafchromic EBT3 model has a satisfactory useful range for radiotherapy applications (Andrés *et al* 2010, Reinhardt *et al* 2012).

Radiochromic films are not standalone dosimetry systems. They have to be used in conjunction with some other device in order to read out the film. A flatbed scanner is the more common choice (Lynch *et al* 2006, Ferreira *et al* 2009). A processing protocol that relates digital signal as read out by the scanner with dose in the film has to be established.

In spite of the many advantages radiochromic film dosimetry presents, it also has several issues that have to be addressed. Radiochromic film dosimetry weaknesses can be associated with non uniformity in the thickness of the active layer of the film, lack of uniformity, the presence of noise in the scanning process or other scanning artifacts (Martišíková *et al* 2008, Richley *et al* 2010, Schoenfeld *et al* 2014, Van Battum *et al* 2015).

The flatbed scanner can produce a color image. It has been common practice to use information coming from just one color channel in the processing protocol, usually the red color one as it has superior sensitivity. Several authors (Alva *et al* 2002, Devic *et al* 2009, Massillon-JL and Zuñiga-Meneses 2010), have used the signals coming from the green and blue channels to extend the dynamic range of the film. To reduce the effects that non uniformity and noise introduce in the processing protocols several methods, which include different scanning pre and post film irradiation, were proposed (Devic *et al* 2005).

Micke *et al* (2011) introduced a multichannel processing protocol that simultaneously combining the information from two or three color channels, it is able to separate a part that is dose-dependent from another one that is dose-independent. It is assumed that the dose-independent part relates with the perturbation caused by non uniformity and by scanner noise, so the dose-dependent part is more robust than the one coming from a single channel protocol.

Mayer *et al* (2012) and Méndez *et al* (2014) have refined the work of Micke by studying the weighted mean dose of all three channels, and Pérez Azorín *et al* (2014) by including explicitly the information provided by the unexposed image of the film. These strategies try to improve the measurement at the cost of increasing the number of film scanning, either pre or post irradiation, but also requires an additional spatial registration with a perfect pixel match between both images. In the same direction of Micke's proposal, a processing protocol based in just one scan would be an advance for radiochromic films to become a handy dosimeter for IMRT quality control.

Denoising algorithms based on non-local means have been used in image processing for the last decade (Buades *et al* 2005b). To reduce the noise in the image, these algorithms replace the color of a pixel with the average of the colors of other pixels that resemble its color, up to the fluctuations due to noise (Buades *et al* 2011). The pixels used in the average calculation may come from anywhere in the image. The main advantage of using these algorithms, is that they can mitigate the noise without relying on multiple images.

The purpose of this paper is to propose a new processing protocol that applies the non-local means algorithm to radiochromic film dosimetry.

2. Method and materials

2.1. Non-local means denoising algorithm

Every observed pixel p of an image $v(p)$ can be expressed as

$$v(p) = u(p) + n(p), \quad (1)$$

where $u(p)$ is the 'true' value and $n(p)$ represents the perturbation due to noise. The aim of a denoising algorithm is to recover the image u .

Let u be defined in a bounded domain $\Omega \subset \mathbb{R}^2$, the non-local means algorithm, as introduced by Buades *et al* (2005a), is defined by replacing $v(x)$ with

$$NL[v](x) = \frac{1}{C(x)} \int_{\Omega} e^{-\frac{f(x,y)}{h^2}} v(y) dy, \quad (2)$$

where $x \in \Omega$, $f(x, y) = \int_{\mathbb{R}^2} G_a(t) |v(x+t) - v(y+t)|^2 dt$, being G_a a Gaussian kernel, $C(x) = \int_{\Omega} e^{-\frac{f(x,z)}{h^2}} dz$ is a normalization factor, y and z are variables of integration over Ω , and h acts as a filtering parameter. Using this expression the denoised value at x is an average of the values of all pixels whose gaussian neighborhood looks like the neighborhood of x .

2.2. Non-local means pixelwise implementation for color images

Consider a color image with three color channels $u = (u_1, u_2, u_3)$. For a pixel p its denoised value produced by the non-local means algorithm is

$$\hat{u}_c(p) = \frac{1}{C(p)} \sum_{q \in B(p,r)} u_c(q) w(p, q), \quad C(p) = \sum_{q \in B(p,r)} w(p, q), \quad (3)$$

where $c \in \{1, 2, 3\}$ and it represents each color channel, and where $B(p, r)$ indicates a neighborhood centered at p with size $(2r+1) \times (2r+1)$ pixels. The patch distance r is the number of pixels to take into account for each image axis and direction. The sums are made over each pixel q belonging to $B(p, r)$.

The weight w is now calculated as

$$w(p, q) = e^{-\frac{\max(d^2 - 2\sigma^2, 0.0)}{h^2}}, \quad (4)$$

where σ is the standard deviation of the noise and h is the filtering parameter. For a patch size s the squared Euclidean distance d^2 in the pixel color space is defined as

$$d^2(B(p,s), B(q,s)) = \frac{1}{3(2s+1)^2} \sum_{c=1}^3 \sum_{j \in B(0,s)} (u_c(p+j) - u_c(q+j))^2. \quad (5)$$

The restored pixel value $\hat{u}_i(p)$ of each pixel and color channel is an average of the most resembling pixels. The smaller the distance $d^2(B(p, s), B(q, s))$, the more a pixel p resembles to a pixel q . To compute resemblance of the two pixels, the algorithm takes into account $(2s+1) \times (2s+1) \times 3$ color values centered at p and q . Each $\hat{u}_c(p)$, no matter the channel c , is the result of the average of the same pixels.

2.3. Non-local means applied to radiochromic film dosimetry

Following equation (1) let $u_c(p)$ be the ‘true’ image of an irradiated radiochromic film. For each p pixel, the three u_c color channel values are not independent, because the radiochromic film physics establishes a relationship between dose and each color channel value. So from a theoretical point of view in the three-dimensional space with coordinates u_c , we can only move over a parametric curve of the dose D , defined by three functions $u_c(D)$.

If we now take into account the noise contribution, in the new image, the point $(v_1(p, D), v_2(p, D), v_3(p, D))$ does not have to lay on the same curve as $u_c(p)$ due to the contribution of $n_c(p)$. $n_c(p)$ sources are variations of the thickness of the active layer of the film, variations of the concentration of monomers in the film, lack of uniformity in the digital scanner, electronic noise and scanning artifacts like dust particles or scratches.

As Micke *et al* (2011) pointed out, radiochromic film provides a different response in each of the three color channels with different slopes of the calibration curves, i.e. the color response vs. dose response curves. Therefore, we must expect that applying the non-local means algorithm to the noisy image, the average of color resembling pixels coming from different areas in the image should mitigate electronic noise and other perturbation sources.

The color response is measured by means of a flatbed scanner. The digital signal it produces in transmission mode is related to light absorption in the film. Light absorption can be quantified by optical density d defined using the digital signal S as

$$d = \log_{10} \frac{2^n}{S}, \quad (6)$$

where n represents S bit depth. For a 48-bit color image, $n = 16$. The optical density d can be expressed as the sum of two contributions, the attenuation of an unexposed film, background optical density d_B , and the light absorption by the polymers created from the reaction induced by the absorbed dose, net optical density d_N . Taking this into account is possible to write

$$d_N = d - d_B = \log_{10} \frac{2^n}{S} - \log_{10} \frac{2^n}{B} = \log_{10} \frac{B}{S}, \quad (7)$$

where B is the digital signal of an unexposed film. There are several options to establish the value of B : at batch level, assuming all the films belonging the same production batch have the same value; at film level, assuming a mean B value for all the pixels in the film; and at pixel level, the value of B varies pixel to pixel. In spite of its apparent superiority the last approach is only useful if fluctuations due to noise are less than background variations.

If the background value is going to be established at batch level, the steps of the processing protocol we propose in this paper are: read out the film as a 48-bit color image in a single scan, apply the non-local means algorithm to the image, split the denoised image into its color channels and apply the corresponding calibration curve to each split denoised image. In this case we could use equation 7 with the values of the background for every color channel B_c determined during calibration.

With background values established at film level the steps would be the same as the previous ones, but an unexposed piece of the film has to be scanned at the same time as the irradiated film. The background value for every color channel has to be updated with the current measured values.

For background values established at pixel level, the steps of the processing protocol would be: digitize the unexposed film, a 48-bit color depth single scan, denoise it by using the non-local means algorithm, irradiate and wait the time to minimize post-exposure change errors, digitize the exposed film and denoise it, split both images into their color channels and apply the corresponding calibration curves using the d_N definition.

Either way these processing protocols produce three dose images \hat{u}_c , one for each color channel c . Applying equation (1) to a color image we can get one estimation of the noise in each channel as

$$\hat{n}_c(p) = v_c(p) - \hat{u}_c(p), \quad (8)$$

where $v_c(p)$ is the value of the pixel p in the split image of the color channel c . One difference between our processing protocol and those ones derived from Micke’s work is that we get three maps \hat{n}_c while they assume a single map of channel-independent perturbations.

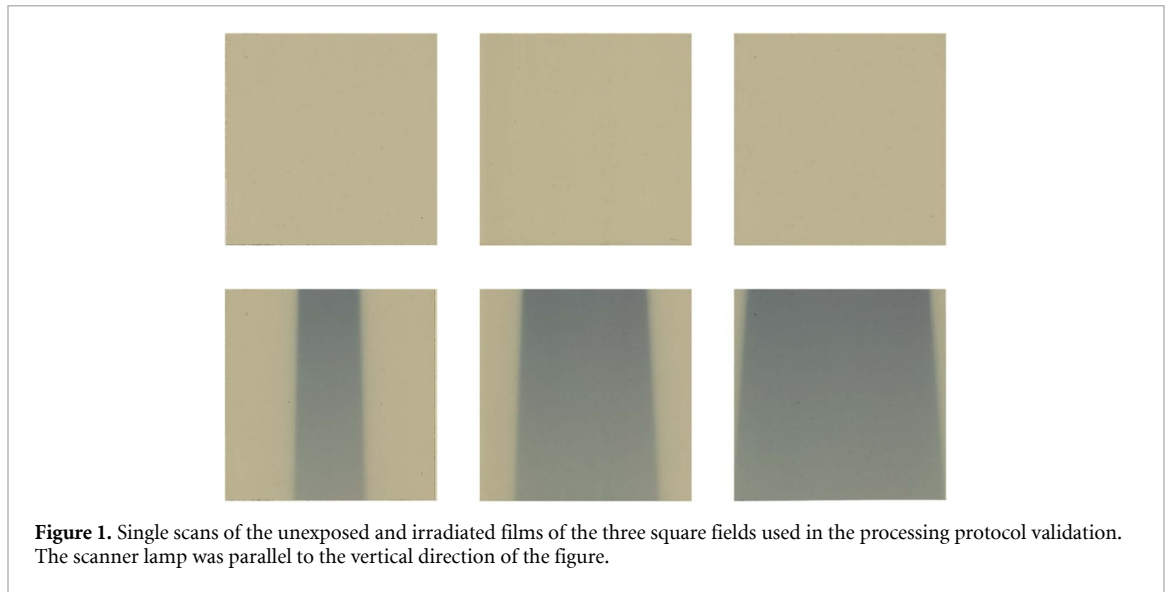


Figure 1. Single scans of the unexposed and irradiated films of the three square fields used in the processing protocol validation. The scanner lamp was parallel to the vertical direction of the figure.

The parametric relationship we have chosen to use as calibration curve in this work is a fitting function with qualitative behaviour similar to film (Lewis *et al* (2012):

$$d_N = \log_{10} \frac{\alpha + \beta D}{\gamma + D}. \quad (9)$$

As we obtain three different images, we can infer three different doses D_c , each of them from the corresponding color channel. These D_c doses are representations of the same ‘true’ dose image. In principle, any combination of the three doses could be used as an estimation of the dose. A reasonable choice is to use the weighted average of the three as follows:

$$D(p) = \frac{1}{W} \sum_c W_c D_c(p), \quad (10)$$

where D_c is the inferred dose from the channel c , W_c is the weight for the channel c and $W = \sum_c W_c$. The W_c values were taken as the inverse of the square of the average estimated uncertainties of D_c .

The collection of image processing algorithms implemented in the Python programming language named *scikit-image* (Van der Walt *et al* 2014) has been employed to make our calculations. This software package includes two versions of the non-local means algorithm, the original following Buades *et al* (2011) and a fast version (Darbon *et al* 2008). We have used the fast implementation with a patch size of 3 pixels and a patch distance of 10 pixels. The filtering parameter was set to be $h = 0.05$ in equation 4. These parameters were chosen to balance computation time, image denoising, and blurring.

2.4. Processing protocol validation

2.4.1. Open square fields

The protocol is validated by measuring well-determined absorbed dose spatial distributions using EBT3 films coming from the same production batch. Three open square fields have been measured by means of radiochromic films and their results compared with their dose distributions calculated by an Acuros XB algorithm in a Varian Eclipse radiotherapy planning system (RTPS). Acuros XB is a dose calculation algorithm based on a deterministic solution of the linear Boltzmann transport equations. The algorithm has been validated (Yan *et al* 2017) and its calculations for open 6 MV photon beams on homogeneous phantoms were within 1% of measurements made with ionization chambers. The unexposed films were scanned first and then irradiated in a linear accelerator Siemens Artiste. The nominal energy of the photon beam was 6 MV. The square field sides were 5, 10 and 15 centimeters. Each film was placed inside an IBA Dosimetry I’mRT phantom of RW3 material. The source surface distance was 90 centimeters and the film was parallel to the beam axis. The measurements were done with a number of monitor units intended to get a dose range between 1.25 and 3.75 Gy.

Twenty four hours after irradiation the films were scanned in a Microtek ScanMaker 1000 XL. As orientation of film portrait was chosen. The scanned images, both unexposed and irradiated films, were 72 dpi in spatial resolution and its digital signal was 48 bits in depth, 16 bits each color channel. Any automatic correction applied by the scanning process was switched off. As proposed in our method, a single

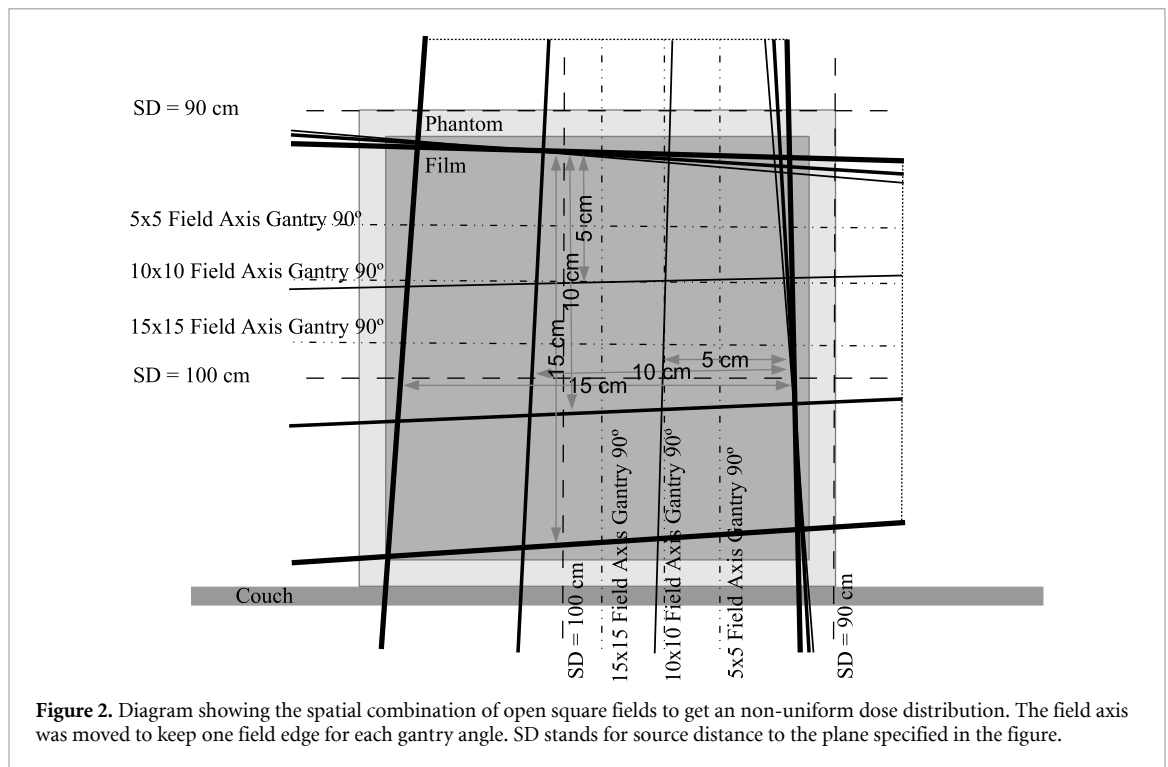


Figure 2. Diagram showing the spatial combination of open square fields to get a non-uniform dose distribution. The field axis was moved to keep one field edge for each gantry angle. SD stands for source distance to the plane specified in the figure.

scan was done. In figure 1 the scanned images with unexposed films and three fields are shown. The calibration curve was previously established for the production batch. To do so, 12 film cut out patches, $1.5 \text{ cm} \times 16 \text{ cm}$ in size were used. They were irradiated in the center of a $20 \text{ cm} \times 20 \text{ cm}$ square beam, 6 MV nominal energy, 10 cm depth and 90 cm source film distance inside the phantom. Each piece was irradiated with a uniform absorbed dose of 0.75, 1.25, 1.75, 2.25, 2.75, 3.25, 3.75, 4.25, 6, 8, and 10 Gy and one of them was left without being irradiated. These film patches were scanned under the same conditions previously explained. For each patch and color channel, the digital signal average of a central region, $1.0 \text{ cm} \times 3.0 \text{ cm}$ in size, was considered to build the calibration curve, equation (9). For each color channel, the standard deviations of the digital signal in these regions were calculated and used as input into our uncertainty estimation.

Using the method proposed in this work and the images shown in figure 1, the spatial distribution of the absorbed dose was obtained. The depth dose curve of the central axis for each square field was extracted. These curves were compared with those calculated using the Acuros XB algorithm. The comparison was carried out using the 1D gamma index with 3% global dose and 3 mm distance criteria, and 0.3 Gy dose threshold. As all other gamma index calculations carried out in this paper, it was calculated using the Gamma Index module of PyMedPhys, a Python package of useful tools in the field of medical physics. Additionally, the local percent dose difference was calculated for every pixel in the dose image relative to the calculated dose value. Since the dose distributions are produced by simple static fields, the difference between the observed and measured doses is directly related to the uncertainty of our protocol.

2.4.2. Non-uniform dose distribution

To get a non-uniform dose distribution a spatial combination of the three previously described open fields was used. The source surface distance was 90 centimeters. Two angle incidences were chosen, 0 and 90 degrees. The fields were arranged as shown in figure 2.

The absorbed dose measurements were compared with the Acuros XB algorithm calculations by means of the 2D gamma index with 3% global dose and 3 mm distance criteria, and 0.3 Gy dose threshold. As described in the previous section, the dose distribution is produced by static and simple fields, so the relative dose difference distribution was computed as well and used for our protocol dose uncertainty determination.

2.4.3. Simulation of an IMRT dose distribution perturbed by scanning lateral artifact and noise

To evaluate the ability of the non-local means protocol to mitigate the scanning lateral artifact with or without the presence of noise we have simulated a realistic dose distribution, using as a starting point the calculated dose $D(x, y)$ in a sagittal plane of a head and neck IMRT actual treatment. A scanning lateral artifact was introduced following Menegotti *et al* (2008) as a function of the dose, with a spatial parabolic

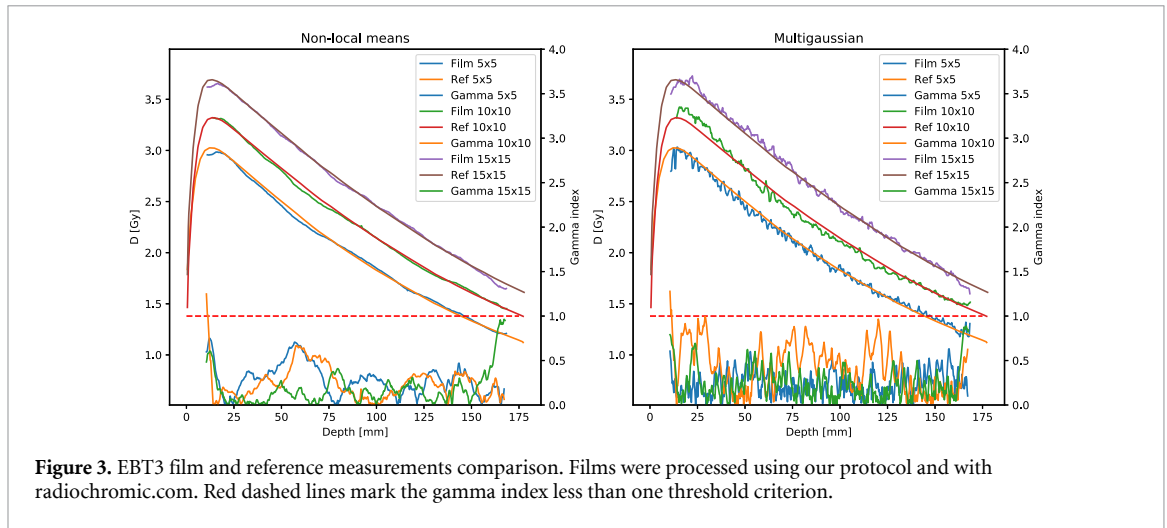


Figure 3. EBT3 film and reference measurements comparison. Films were processed using our protocol and with radiochromic.com. Red dashed lines mark the gamma index less than one threshold criterion.

dependence as follows:

$$L(D, x) = 1 + (c_0 + c_1 \cdot D + c_2 \cdot D^2) \cdot x^2, \quad (11)$$

where x represents the corresponding pixel coordinate considering the origin in the center of the image. In this paper we have considered $c_0 = -1.07 \cdot 10^{-6}$, $c_1 = -3.72 \cdot 10^{-6}$ and $c_2 = 3.39 \cdot 10^{-7}$ when x is measured in millimetres. These values were selected to produce a maximum lack of uniformity ranging from 2% to 6% when the dose varies from 0.5 Gy to 3 Gy.

Then, the non-uniform dose distribution is

$$D_p(x, y) = D(x, y) \cdot \{1 + [c_0 + c_1 \cdot D(x, y) + c_2 \cdot D(x, y)^2] \cdot x^2\}. \quad (12)$$

Combining equations (7) and (9) the corresponding noise-free signals $\tilde{v}_c(x, y)$ for every color channel c were computed. The values of the background digital signals were fixed to those measured during batch calibration. To introduce random noise in the signal, the values of $\tilde{v}_c(x, y)$ were replaced by

$$v_c(x, y) = \tilde{v}_c(x, y) \cdot [1 + N(\sigma_c)], \quad (13)$$

where N represents a random variable following a normal distribution with a mean value of 0 and a standard deviation of $\sigma_r = 0.006$ for the red channel, $\sigma_g = 0.009$ for the green channel, and $\sigma_b = 0.012$ for the blue channel.

The simulated signals v_c were processed using the non-local means protocols. Additionally, the red color signals were processed as well with the single-channel protocol. The calculated doses were compared with the reference dose $D(x, y)$ and the relative dose difference expressed as a percentage of $D(x, y)$ was evaluated.

2.5. Comparison with a commercial implementation of the multichannel protocol

The images of the three open square field dose distributions and the spatial combination of open square fields were processed as well using the implementation of the multichannel protocol provided by the web application radiochromic.com, the so-called *multigaussian method* (Mendez *et al* 2018). To establish the calibration curve with the tools this application provides, the same data used with our processing method was employed. To measure the dose distributions, the protocols explained in the step by step tutorials on the radiochromic.com site were followed. The average of five scans of unexposed films and the average of other five scans of the irradiated film for each dose distribution were employed in the analysis. The advance options provided by the application were used: noise reduction by means of a median filter with a window of five pixels; inter-scan correction using an unexposed film kept in a fixed position since the batch calibration was carried out. The same parameters calculated using the non-local means protocol were determined as well with the multigaussian method.

3. Results and discussion

3.1. Open square fields

Figure 3 shows the validation of the non-local means processing protocol by means of the comparison of open square field depth dose curves analysed using both protocols. A quantitative comparison based on the gamma index is shown as well.

Table 1. Gamma index results for square open fields. Global stands for the statistics of all fields.

Field	Non-local means		Multigaussian	
	$\bar{\gamma}$	$\gamma < 1$	$\bar{\gamma}$	$\gamma < 1$
5 × 5	0.28	100%	0.24	100%
10 × 10	0.24	99.3%	0.42	99.3%
15 × 15	0.18	100%	0.24	100%
Global	0.23	99.7%	0.30	100%

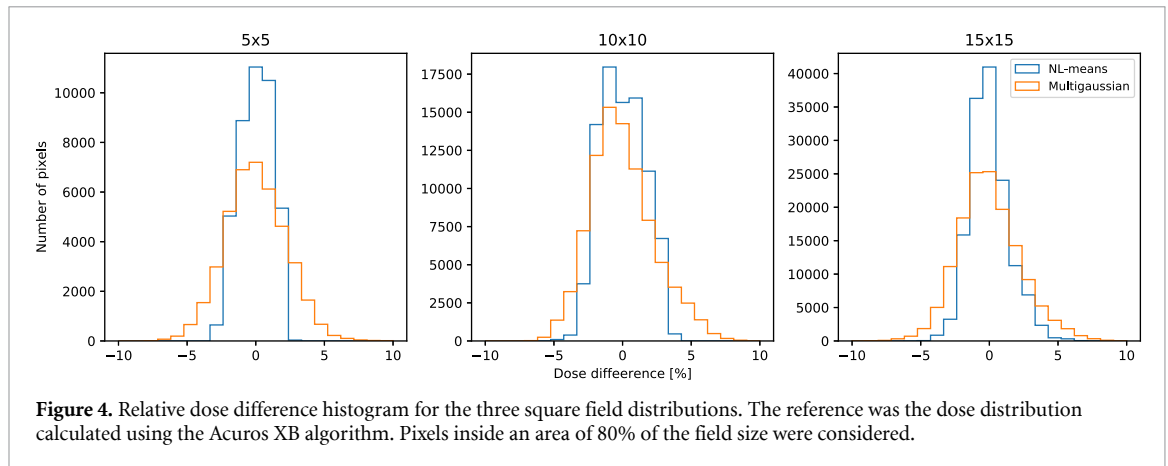


Table 1 shows the mean values of the gamma analysis and the number of pixels percentage with gamma index inferior to 1. The worst result is for the 10 × 10 field for which we get that at least 99.3% of the analyzed pixels have a gamma index inferior to 1. The average gamma value is 0.36.

In terms of the spatial distribution, it is possible to see some edge effect in the measured depth dose curve as the gamma index tends to increase its value in an internal ring of about 0.5 cm width around the film edges, even though it is still mostly less than 1 under our criteria. A possible explanation to this edge effect could be some sort of damage due to film handling or a variation in the digital signal associated with light scattering at film edge.

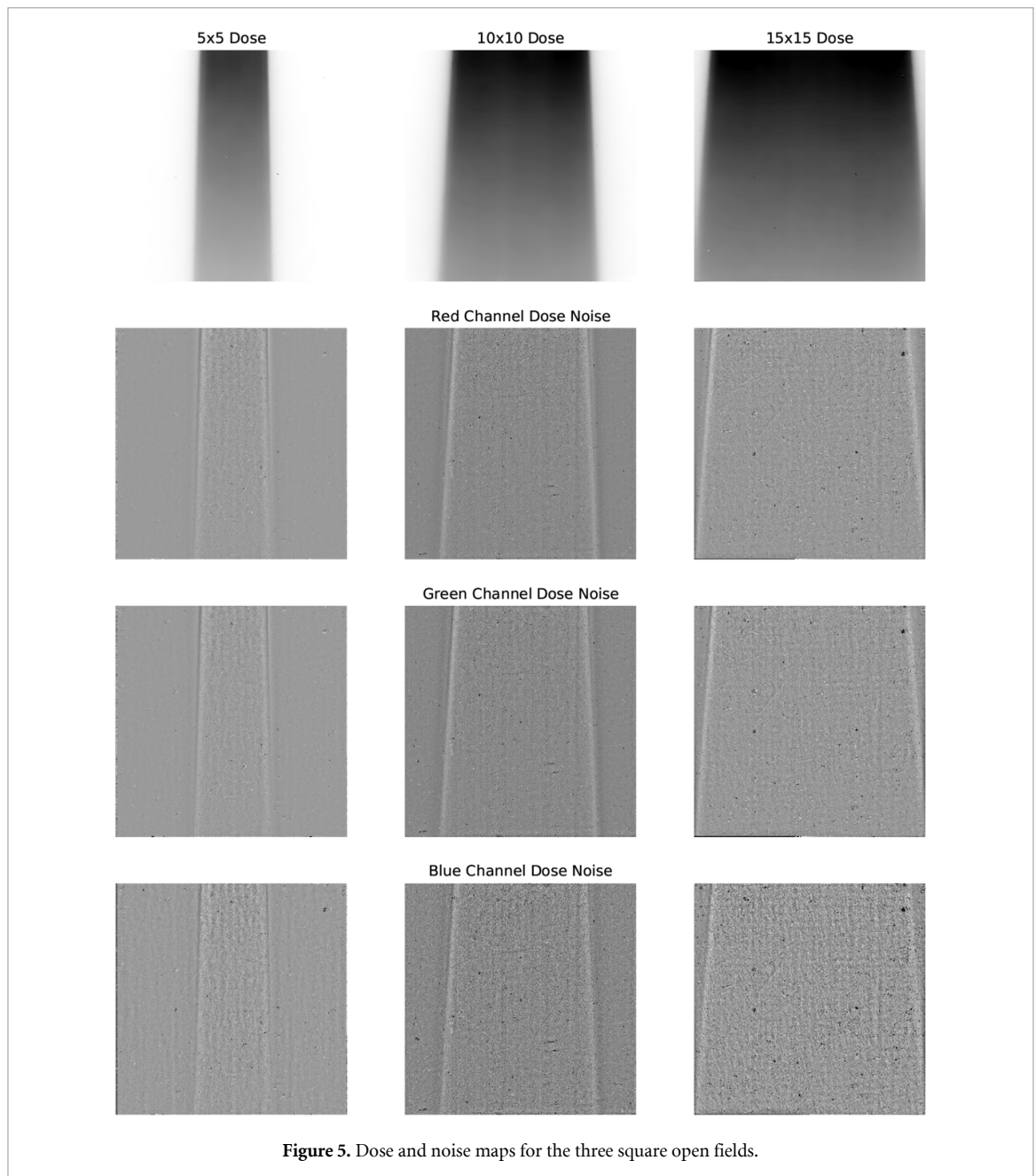
Figure 4 shows the relative dose difference histogram for each open square fields using both protocols. As can be seen in figure 3, the non-local means improves noise suppression without introducing measurement bias, and this is reflected in narrower relative dose difference distributions as shown in figure 4.

The non-local means algorithm is performed in the digital signal space, the dose is only implicitly considered as it establishes a relationship between the three color channel digital signals of each pixel. Figure 5 shows the dose and noise maps obtained using equations (8), (9), and (10) for every color channel. If the noise were completely random in nature, we should expect no recognizable image in the noise maps. Although mostly random, we can identify the field edge and some perturbations that appear at the same location in every map. These located perturbations could be due to dust, smudges or scratches. It can be observed as well that the intensities of the random noise and the located perturbations are different for each color channel. For their part, the multichannel protocols take into account explicitly the calibration curve in the perturbation calculation, producing just one perturbation map.

3.2. Non-uniform dose distribution

Figure 6 shows the reference dose corresponding to a spatial combination of open square fields, traceable to ionization chamber measurements, and the processed dose using the non-local means and the multigaussian algorithms. As can be seen, the non-local means protocol is more efficient than the multigaussian method in the process of denoising the dose distribution; vertical slight fluctuations in the scan direction are still visible in the dose determined by the multigaussian method that are not observable in the non-local means image.

Figure 7 shows the gamma index maps of the comparison of the non-local means vs. the reference dose and the standard multichannel vs. the reference dose. Although mostly similar, both distributions are practically under the $\gamma < 1$ criterion for the whole image, a slightly better result is obtained with non-local means protocol. This can be quantitatively seen in figure 8 where a higher percentage of pixels with gamma value lower than 0.5 is measured using the non-local means protocol. The same that happened with the single square field dose distributions, this combination of conventional fields produces a narrower relative local dose difference. Since the fields used in these measurements are static, the dose-difference histograms



provide a direct determination of the uncertainty for both protocols in the dose range these measurements comprehend.

The uncertainty as a function of the absorbed dose is the combination of two contributions: the calibration uncertainty and the measurement test uncertainty. Under ideal conditions absorbed dose and digital signal are related by a bijective function, but in practice unknown variables like the active layer thickness, density of active elements in the active layer, scratches or dust in the film, lack of uniformity in the light emission or in the scanner detector, change over time of the light intensity in the scanner lamp, electronic noise; all these variables imply that we can measure different digital signals corresponding to the same dose value. During calibration, we determine the response curve which relates the absorbed dose with the digital signal. The uncertainty in this process is reflected by the uncertainty in the determination of the parameters of the calibration curve. The calibration is performed so that these uncertainties are minimized. Large areas of the film could be irradiated with the same dose, so a high number of pixels should provide statistical samples of the same ideal digital signal value. We can average over these samples to get the best estimator of the digital signal to be used in the calibration curve. The standard deviation of these means are used to determine the uncertainty in the calibration curve parameters. During the measurement these large areas are not available, so the standard deviation of the sample should be used to estimate the uncertainty if no further action is taken. To minimize the uncertainty coming from the scanner several scans could be

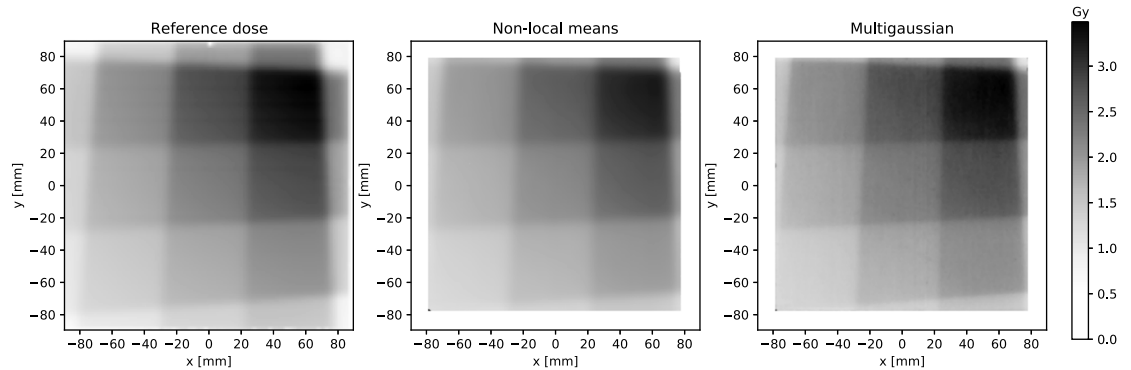


Figure 6. Non-uniform dose distribution test. It should be noted that the I'mRT cube phantom is 180 mm in side, but just a film 160 mm in side can be inserted.

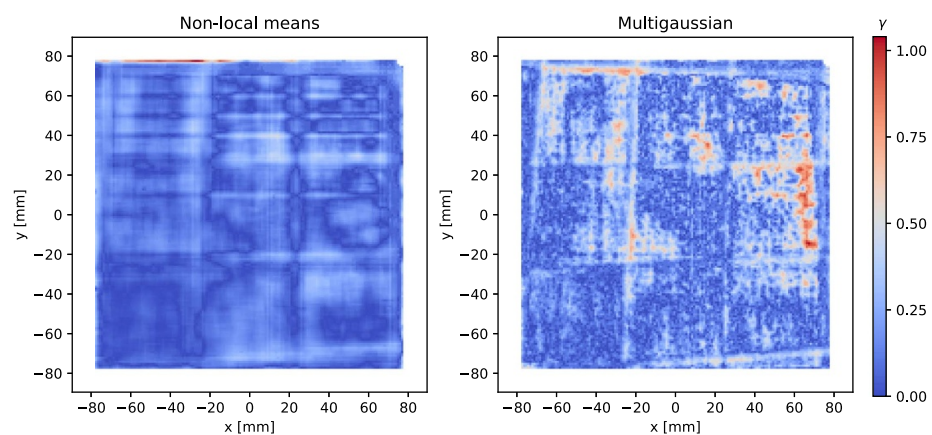


Figure 7. Gamma index spatial distributions for the non-uniform dose test.

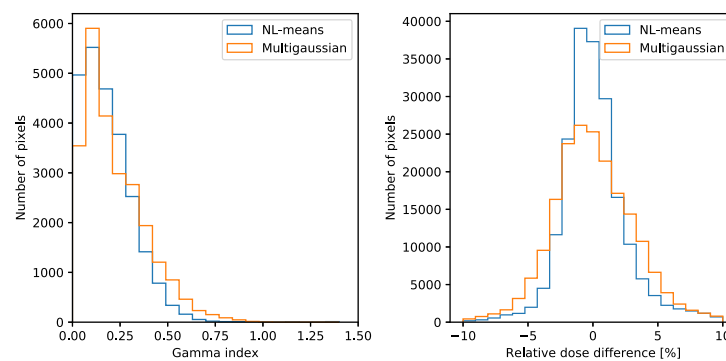


Figure 8. Gamma index and relative local dose difference histograms for the non-uniform dose distribution test.

made, but Devic *et al* (2005) have shown that doing more than five scans does not significantly improve signal measurement reproducibility. Several images using different films could be taken, but this is not a common strategy in practice. The uncertainty in the dose estimates eventually depend on the processing protocol and its final quantification could be a complex issue. Using the methodology proposed by Vera-Sánchez *et al* (2018) we have evaluated the uncertainties on the multigaussian method and on the non-local means protocols. A distinction has to be made between the stages comprising the calibration process and those involving the measurement protocol. Figure 9 shows this evaluation. Combined standard uncertainty is given as a percentage of the the measured absorbed dose. Calibration uncertainties are the same for both protocols, but whereas this uncertainty is just a contribution to total uncertainty of the multichannel protocols, it is the main contribution for the non-local means protocols, due to its superior noise reduction, based on its ability to average several pixels without relying on multiple images.

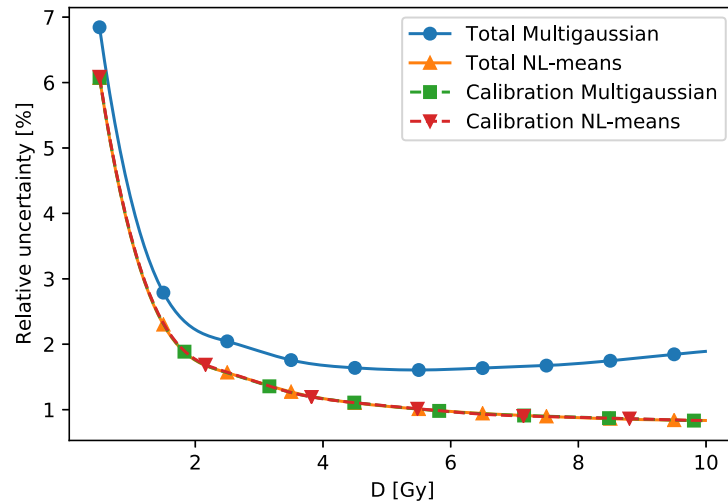


Figure 9. Uncertainty evaluation of both protocols.

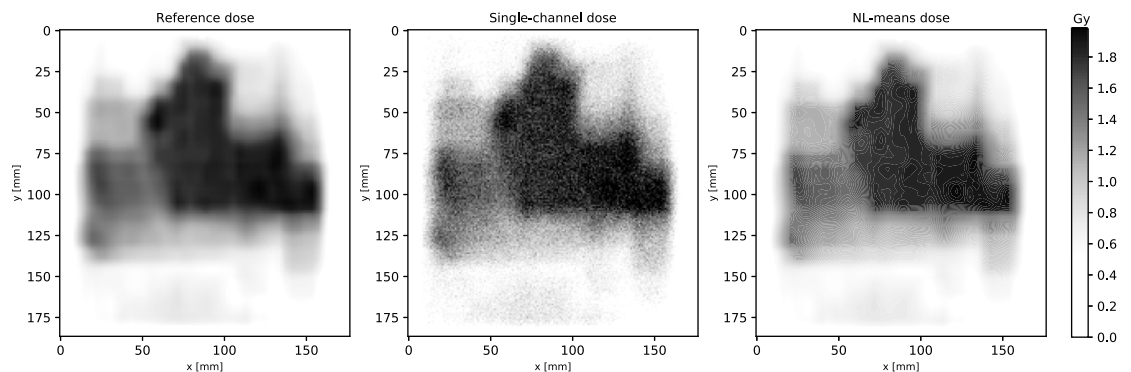


Figure 10. Absorbed dose spatial distributions without perturbation, reference dose, and with simulated scanning lateral artifact and noise processed by the single channel protocol and non-local means protocol.

Considering the dose range in the open square field measurements and in the non-uniform dose test, according to figure 9 we should expect a relative dose difference distribution with a standard deviation of about 2.3% for the multichannel protocol, and about 1.8% for the non-local means protocol, in good agreement with the histograms shown in figures 4 and 8.

3.3. Simulation of an IMRT dose distribution perturbed by scanning lateral artifact and noise

To quantify the ability of the non-local means protocol to mitigate the scanning lateral artifact, we have used the spatial dose distribution of an actual IMRT treatment for a head and neck cancer case. This distribution was perturbed by a specific scanning lateral artifact and by noise to simulate realistic digital signals. This strategy allows us to know the true dose producing the measured digital signal, something unreachable in a real setup measurement. In figure 10 the reference dose, the true dose used in the simulation, is shown. In this figure we can see the recovered dose from the single channel method, using the red channel digital signal, and from the non-local means protocol. The single channel dose would be obtained in the case of no further corrections. It represents the degradation the measurement system introduces if just a bijective relationship between dose and digital signal is considered. An ideal processing protocol should recover the reference dose.

In figure 11 several dose profiles under different simulation conditions and processing protocols are shown. The reference dose has been perturbed by only a scanning lateral artifact and by the combination of a scanning lateral artifact and noise. The digital signals derived from these simulations have been processed by the single-channel and non-local means protocols. The figure shows the dose obtained by the non-local protocol when applied to the simulated digital signal including the lateral artifact and noise.

Figure 12 shows the relative dose difference histograms of the recovered doses under different simulation conditions and processing protocols. On its own, the lateral scanning artifact introduces an uncertainty that the non-local means protocol is able to mostly mitigate in the case of absence of noise. In practice this is not a

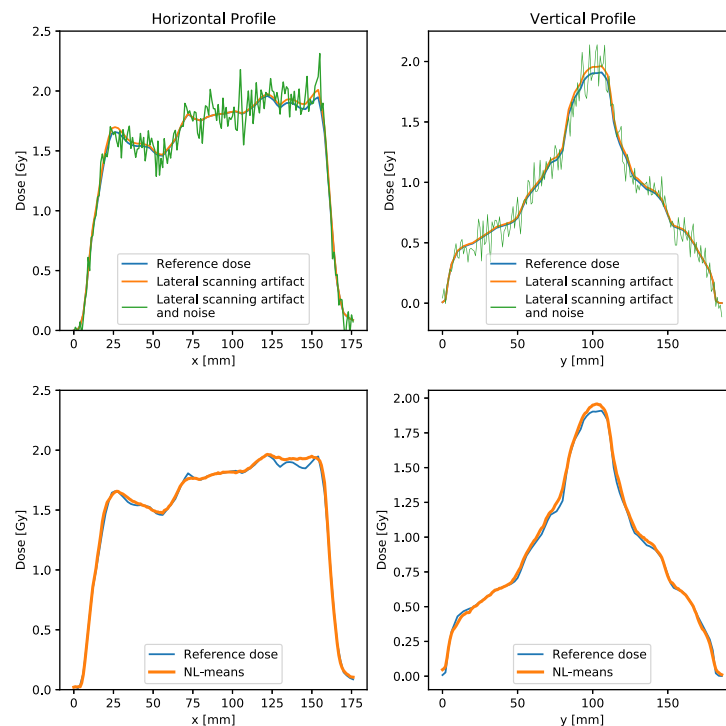


Figure 11. Superior part: Dose profiles under different conditions: without perturbation, reference dose; with simulated scanning lateral artifact; with simulated scanning lateral artifact and noise. Inferior part: Reference dose profiles comparison with the ones obtained using the non-local means in the simulated signals with scanning lateral artifact and noise.

realistic situation, as the artifact will always appear in combination with measurement noise, the main source of measurement degradation, see the dose difference histogram of scanning lateral artifact and noise processed with the single channel protocol. Under combined lateral artifact and noise the non-local means protocol is able to mostly suppress the noise and partly mitigate the scanning lateral artifact, its uncertainty being similar to that of the simulation of just lateral scanning artifact. The non-local means protocol redistribute the mitigated lateral artifact over the entire image area, as can be seen in figure 11.

Being able to mitigate perturbations without relying on multiple images is the main strength of the non-local means protocol. For every test we have used five scans of the unexposed film and other five scans of the irradiated film to be processed with the multichannel protocol, whereas one single scan of the unexposed film and another one of the irradiated film were used with the non-local means protocols. In spite of the reduction in the scan number, non-local means results show an improving performance in relation to the multigaussian method results.

In this paper we have considered the optical density of the unexposed film at the pixel level. The decision to do so was made following the recommended protocols on radiochromic.com website, as we wanted to get the better results the application could produce. This approach implies two scan series, pre and post irradiation, and a spatial registration of both series. Assuming a slightly increased uncertainty, it is possible to drop the unexposed film scans of the processing protocol using the background value determination at film or batch level. The non-local means protocol still improves the results of the multigaussian protocol with background determination at pixel level. We estimate a combined standard uncertainty of 2.1% for non-local means with background established at film level whereas 2.3% was estimated for the multigaussian method with background values considered at pixel level.

The non-local means algorithm parameters depend on the measurement arrangement, particularly on the scanning resolution and the level of noise. The parameters given in this paper are not expected to be valid under different configurations and could be considered just like an initial suggestion to other settings. The value of the h parameter should be determined according to the level of noise and it could vary with the image pixel size (Massillon-JL and Zuñiga-Meneses 2010). The patch size and patch distance should be scaled according to scanning resolution set in the measurement.

Radiochromic film dosimetry is intended for measuring spatial absorbed dose distributions and it might seem unnatural to average signals that could come from other locations on the image, because there would be a risk of losing the image spatial information and altering the dose distribution. It is important to point out that the metrics of the non-local means algorithm just selects pixels that are considered similar, taking

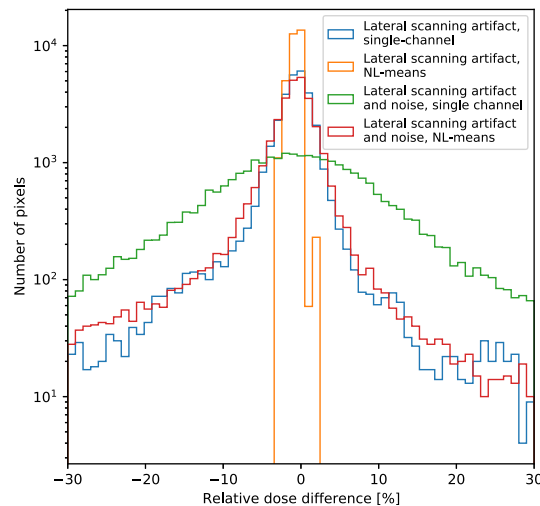


Figure 12. Relative dose difference histograms for the IMRT head and neck cancer treatment under different simulation conditions and processing protocols.

into account the pixel itself and the pixels around it. Bearing in mind that the radiation energy deposition mechanisms imply some correlation between each pixel and its surroundings, i.e. the inherent spatial resolution of a dose distribution produced from a radiotherapy external beam is limited to a few millimeters, an area covered by several pixels, and that there is a correlation between the color channel digital signal of each pixel imposed by the physics of the light attenuation in the radiochromic film active layer, it should be possible to select the proper parameters to configure the non-local means algorithm to mitigate perturbations without compromising the ability of the radiochromic films to record the actual dose distribution. The set of open square fields combined to produce a non-uniform dose distribution was designed to test this issue. Figure 6 includes areas of nearly uniform dose, separated by zones of high dose gradients; as shown in figures 6 and 7, the results of the non-local protocol do not shift dose values between different areas, and the spatial resolution in the high gradient zones is at least as good as that of the multigaussian method.

The multichannel characteristics of non-local means protocol takes advantage of the different slopes the calibration curve has for every color channel. In recent years flat-bed scanner manufacturers have started to replace cold cathode fluorescent lamps with LED lamps. The digital signal the scanner produces in transmission mode is the combination of three elements: the scanner lamp spectrum, the film absorbance curve and the response of the scanner detector array. Therefore, the change in the light emitted has to imply a different relationship between the signal coming from each color channel, but different responses are still expected as the absorbance curve is different in each color band. The results shown in this paper have been obtained using a scanner with a cold cathode fluorescent lamp. Work should be done in the future to check if the proposed protocol is useful with LED scanners.

4. Conclusions

A new processing protocol for radiochromic film dosimetry based on non-local means has been presented. The dose measurement using this protocol has been validated in three general situations: square open field dose distributions, non-uniform dose distributions with doses ranging from 1 to 4 Gy, and a highly modulated dose distribution corresponding to a clinical treatment in which we have simulated the scanning lateral artifact and the presence of noise. These measurement and simulation situations have been chosen because the dose taken as reference to validate the protocol can be known with a high level of confidence. Our results indicate that this processing protocol could be employed to measure dose distributions produced in external beam radiotherapy treatments. A comparison with the results of an implementation of the multichannel protocol shows that the non-local protocol gives smaller uncertainties, even though it uses fewer scans. The main strength of the proposed protocol is the reduction in absorbed dose measurement uncertainties due to its ability to suppress noise without comprising spatial resolution and without relying on multiple images. This protocol can partly mitigate the scanning lateral artifact, the degree of mitigation depending on the image random noise level.

ORCID iDs

César Rodríguez  <https://orcid.org/0000-0003-3323-7066>

Diego García-Pinto  <https://orcid.org/0000-0003-1348-6735>

References

- Alva H, Mercado-Uribe H, Rodríguez-Villafuerte M and Brandan M 2002 The use of a reflective scanner to study radiochromic film response *Phys. Med. Biol.* **47** 2925
- Andrés C, Del Castillo A, Tortosa R, Alonso D and Barquero R 2010 A comprehensive study of the Gafchromic EBT2 radiochromic film. A comparison with EBT *Med. Phys.* **37** 6271–8
- Buades A, Coll B and Morel J M 2005a Image denoising by non-local averaging *Acoustics, Speech and Signal Processing, 2005. Proc. (ICASSP'05). IEEE Int. Conf. IEEE* vol 2 pp ii–25
- Buades A, Coll B and Morel J M 2005b A non-local algorithm for image denoising *Computer Vision and Pattern Recognition, 2005. CVPR 2005. IEEE Computer Conf. IEEE* vol 2 pp 60–5
- Buades A, Coll B and Morel J M 2011 Non-local means denoising *Image Process. Line* **1** 208–12
- Darbon J, Cunha A, Chan T F, Osher S and Jensen G J 2008 Fast nonlocal filtering applied to electron cryomicroscopy *Biomedical Imaging: From Nano to Macro, 2008. ISBI 2008. 5th IEEE Int. Symp. IEEE* pp 1331–4
- Devic S, Seuntjens J, Sham E, Podgorsak E B, Schmidtlein C R, Kirov A S and Soares C G 2005 Precise radiochromic film dosimetry using a flat-bed document scanner *Med. Phys.* **32** 2245–53
- Devic S, Tomic N and Lewis D 2016 Reference radiochromic film dosimetry: review of technical aspects *Phys. Med.* **32** 541–56
- Devic S, Tomic N, Soares C and Podgorsak E 2009 Optimizing the dynamic range extension of a radiochromic film dosimetry system *Med. Phys.* **36** 429–37
- Ferreira B, Lopes M and Capela M 2009 Evaluation of an Epson flatbed scanner to read Gafchromic EBT films for radiation dosimetry *Phys. Med. Biol.* **54** 1073
- Lewis D, Micke A, Yu X and Chan M 2012 An efficient protocol for radiochromic film dosimetry combining calibration and measurement in a single scan *Med. Phys.* **39** 6339–50
- Lynch B D, Kozelka J, Ranade M K, Li J G, Simon W E and Dempsey J F 2006 Important considerations for radiochromic film dosimetry with flatbed CCD scanners and EBT Gafchromic® film *Med. Phys.* **33** 4551–6
- Martišková M, Ackermann B and Jäkel O 2008 Analysis of uncertainties in Gafchromic® EBT film dosimetry of photon beams *Phys. Med. Biol.* **53** 7013
- Massillon-JL G and Zuñiga-Meneses L 2010 The response of the new MD-V2-55 radiochromic film exposed to 60Co gamma rays *Phys. Med. Biol.* **55** 5437
- Mayer R R, Ma F, Chen Y, Miller R I, Belard A, McDonough J and O'Connell J J 2012 Enhanced dosimetry procedures and assessment for EBT2 radiochromic film *Med. Phys.* **39** 2147–55
- Mendez I, Polšák A, Hudej R and Casar B 2018 The multigaussian method: a new approach to mitigating spatial heterogeneities with multichannel radiochromic film dosimetry *Phys. Med. Biol.* **63** 175013
- Menegotti L, Delana A and Martignano A 2008 Radiochromic film dosimetry with flatbed scanners: A fast and accurate method for dose calibration and uniformity correction with single film exposure *Med. Phys.* **35** 3078–85
- Micke A, Lewis D F and Yu X 2011 Multichannel film dosimetry with nonuniformity correction *Med. Phys.* **38** 2523–34
- Méndez I, Peterlin P, Hudej R, Strojnik A and Casar B 2014 On multichannel film dosimetry with channel-independent perturbations *Med. Phys.* (Wiley Online Library) **41** 011705
- Niroomand-Rad A et al 1998 Radiochromic film dosimetry: recommendations of AAPM radiation therapy committee task group 55 *Med. Phys.* **25** 2093–115
- Pérez Azorín J F, Ramos García L I and Martí-Climent J M 2014 A method for multichannel dosimetry with EBT3 radiochromic films *Med. Phys.* (Wiley Online Library) **41** 062101
- Reinhardt S, Hillbrand M, Wilkens J and Assmann W 2012 Comparison of Gafchromic EBT2 and EBT3 films for clinical photon and proton beams *Med. Phys.* **39** 5257–62
- Richley L, John A, Coomber H and Fletcher S 2010 Evaluation and optimization of the new EBT2 radiochromic film dosimetry system for patient dose verification in radiotherapy *Phys. Med. Biol.* **55** 2601
- Schoenfeld A A, Poppinga D, Harder D, Doerner K J and Poppe B 2014 The artefacts of radiochromic film dosimetry with flatbed scanners and their causation by light scattering from radiation-induced polymers *Phys. Med. Biol.* **59** 3575
- Van Battum L, Huizenga H, Verdaasdonk R and Heukelom S 2015 How flatbed scanners upset accurate film dosimetry *Phys. Med. Biol.* **61** 625
- Van der Walt S, Schönberger J L, Nunez-Iglesias J, Boulogne F, Warner J D, Yager N, Gouillart E, Yu T and the scikit-image contributors 2014 scikit-image: image processing in Python *PeerJ* **2** e453
- Vera-Sánchez J A, Ruiz-Morales C and González-López A 2018 Monte carlo uncertainty analysis of dose estimates in radiochromic film dosimetry with single-channel and multichannel algorithms *Phys. Med.* **47** 23–33
- Villarreal-Barajas J and Khan R 2014 Energy response of EBT3 radiochromic films: implications for dosimetry in kilovoltage range *J. Appl. Clin. Med. Phys.* **15** 331–8
- Yan C, Combine A G, Bednarz G, Lalonde R J, Hu B, Dickens K, Wynn R, Pavord D C and Saiful Huq M 2017 Clinical implementation and evaluation of the Acuros dose calculation algorithm *J. Appl. Clin. Med. Phys.* **18** 195–209